RSC Advances

PAPER

View Article Online
View Journal | View Issue

Cite this: *RSC Adv.*, 2022, **12**, 24640

Fabrication of ballpoint-ink *via* encapsulating inorganic pigments in microemulsion gels

Deski Beri, *[a] Septian Budiman,[a] Nofi Yendri Sudiar,[b] Alfajri Yusra,[c] Erianjoni Erianjoni,[c] Ganefri Ganefri[d] and Ali Amran[a]

The fabrication of ballpoint-ink might open up a new perspective on physico-chemical solubility thermodynamics. In this report, we present a method to encapsulate inorganic pigments, such as $Fe(CNS)_3$ (red), $Fe_2Fe(CN)_6$ (blue), CdS (yellow), and CuS (black) into w/o microemulsion gels. The area of w/o microemulsions was first determined by titrating surfactants Tween-60 into the given composition of water and cyclohexane in the pseudo-three phase diagram. Three prosperous phase areas were successfully mapped using this method, namely: microemulsion (w/o, and o/w) or (μE), lamellar liquid crystal (L_α), and hexagonal liquid crystal (H_α), respectively. The results show that inorganic pigments were well soluble in the w/o microemulsion gel of the Tween-60/cyclohexane/water system. The highest solubility of inorganic pigments in the microemulsion gel is 3.63 ± 0.05 mg g^{-1} for the red pigment of $Fe(CNS)_3$, and the lowest is 2.92 ± 0.05 mg g^{-1} for the yellow pigment of CdS. Hence, the solubility limit distribution for all pigments is 2.9 ± 0.05 <S>3.63 ± 0.05 mg g^{-1}. The cation and anion size strongly affected the inorganic pigments' solubility in the w/o-microemulsion system. Some quantity of the ink-made of inorganic pigments encapsulated in the microemulsion gel has been inserted into empty ballpoint sleeves as prototypes. The resulting self-made inks demonstrated that the physical appearances of the ink could mimic the factory-made inks. Nevertheless, the self-made ink should be investigated further for long lifespan use, especially for long-term stability and corrosion resistance.

Received 19th July 2022
Accepted 19th August 2022

DOI: 10.1039/d2ra04463c

rsc.li/rsc-advances

1 Introduction

The solubility of inorganic substances/transition metal salts in a microemulsion is of great interest because of their outstanding scientific and industrial value.[1] Various inorganic salts have been used as auxiliaries in the textile and dyeing industries for several centuries.[2–4] Nowadays, indigo obtained from inorganic salts has not lost its importance because it offers better stability, especially oxidation resistance, compared with organic pigments.[5] However, research on the solubility of inorganic compounds might play an essential role to unlock the physical and chemical aspects of thermodynamics and kinetics of the molecules microscopically, hence this understanding may be helpful for future advanced research, such as in nanotechnology,[6–8] nanophotonics,[9] nanocoatings,[10] solar cell fabrication,[11] membrane therapy,[12] drug delivery to cancer cells, anti-counterfeiting material coatings,[13] optical sensors,[14] *etc.* In addition, the dissolution of inorganic pigments into microemulsions potentially has a bright future, as it can be applied in the pharmaceutical industry and in the conversion of light into energy, solar cells, sensor technology, and photonics.[15]

Due to their polarity, inorganic pigments have better dissolution properties compare with their cousins called organic pigments.[16] In aqueous solutions, inorganic pigments stick nicely in the water in the presence of surfactants. The head groups find it counters more quickly in the dispersion and are more dispersible than organic dyes.[17] In w/o microemulsions, oil groups are surrounded by the cell-contained packs of inorganic pigments-due to high water solubility. The thermodynamics solubility of inorganic pigments in the w/o microemulsions serve valuable information for physics and chemistry because such a phenomenon can be applied in nanoscale materials synthesis *via* nanoemulsions.[18] This compact dispersion structure enables a long stability dispersion, allowing the production of long-lifespan printing inks and paints.[19] The corresponding advantage of inorganic pigments is, of course, their resistance to oxidation and photolysis. In addition, it is also possible to synthesize nanomaterials with super electrical, magnetic, and optical properties.[20]

Recently, yellow ink-jet ink nano-TiO_2–Sb–Ni was prepared by Talavar, *et al.*[21] using surfactant size control microemulsions.

[a]*Chemistry Department, Faculty of Mathematics and Science, Universitas Negeri Padang, Jl. Hamka, Air Tawar, Padang, Indonesia, 25132. E-mail: deski.beri@fmipa.unp.ac.id*

[b]*Physics Department, Faculty of Mathematics and Science, Universitas Negeri Padang, Jl. Hamka, Air Tawar, Padang, Indonesia, 25132*

[c]*Sociology Department, Faculty of Social Science, Universitas Negeri Padang, Jl. Hamka, Air Tawar, Padang, Indonesia, 25132*

[d]*Electrical Engineering Department, Faculty of Engineering, Universitas Negeri Padang, Jl. Hamka, Air Tawar, Padang, Indonesia, 25132*

The authors claimed that they could produce 65 nm size yellow nanoparticles of Ti/Sb pigment, used for ceramic tiles inks. Nano-TiO_2–Sb–Ni was first encapsulated in the w/o microemulsions to control the size then dissembling and redisperse the material in the surfactant/cosurfactant/water to fabricate the inks.[21] Next, Wang, *et al.*[22] synthesized Pr–$ZrSiO_4$ pigment *via* the sol–gel-microemulsion method, where ZrO_2 and SiO_2 sols are used as water phases, cyclohexane serves as oil phase, and Triton X-100 and 1-hexanol used as surfactant and co-surfactant, respectively. The results show that the materials were ready to be used as ink-jet ink due to the direct transformation of liquid/liquid to solid/liquid interface from sol to gels without emulsifiers' assistance.[22]

In this work, we would like to fabricate ballpoint ink from encapsulated inorganic pigments in the w/o microemulsions gel of Tween-60/cyclohexane/water. This research aims to understand the solubility properties of inorganic pigments in the w/o microemulsions gels and potential applications in the industries. This research can be implemented in chemistry, biology, pharmacy, food sciences, paint, and ink technology.

2 Material and methods

The materials used in this study were freshly prepared inorganic pigments/dyes such as $Fe(CNS)_3$ (red), $Fe_2Fe(CN)_6$ (blue), CdS (yellow), and CuS (black). Surfactant Tween-60 96% purity from Merck (Fig. 1), cyclohexane 98% purity from Merck, tetraethyl orthosilicate (TEOS) 98% from Sigma-Aldrich, ethanol 98% purity from Merck, double distilled water, $Fe(NO_3)_3$ 96% purity from Acros Chem., KSCN 98% purity from Merck, $K_4[Fe(CN)_6]$ 98% purity from Merck, $FeSO_4$ 98% purity, HCl 36% pro analyses from Merck, $CaCl_2$ 98% from Acros Chem., $CuSO_4$ 98% from Merck, FeS 98% from Merck. All pigments were synthesized freshly in the laboratory using known procedures.

2.1 Pseudo-phase diagram of water-Tween-60-cyclohexane

Room temperature pseudo-phase diagram of oil in water and water in oil microemulsions (o/w-μE, & w/o-μE), lamellar liquid crystals (L_α), and hexagonal liquid crystals (H_α) determined by titrating cyclohexane (C6) into the fixed composition of water (W) and Tween-60 (Tw-60) according to the relation 1:

$$X_{Tot} = [x_w + x_{Tw} + x_{C6}] \quad (1)$$

Where $X_{Tot} = 0.50$ g, x_w = weight in % of water, x_s = weight in % of a surfactant, and x_{C6} = weight in % of cyclohexane.

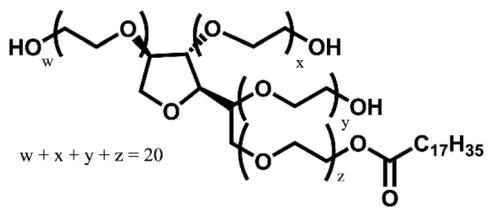

Fig. 1 Molecular Structure of Tween-60 (Tw-60).

The phase boundary was determined carefully by visually investigating sample turbidity after vigorous stirring and shaking at room temperature (25–26 °C). Two-phase liquid with a clear boundary or cloudy mixture was grouped as coarse dispersion and discarded, whereas the clear, transparent, and translucent solution was grouped as microemulsions. Depending on the phase continuity and the position in the diagrams, the microemulsions were grouped as oil-in-water microemulsion (o/w-μE), and water-in-oil microemulsion (w/o-μE).

Next, to distinguish μE and liquid crystals, two parafilm plates were used to observe the light polarizability. The ability to rotate polarized light is the strong signature of liquid crystalline materials. There were two types of liquid crystals, namely lamellar/smectic liquid crystals (L_α) and hexagonal liquid crystals (H_α). To distinguish between L_α and H_α-phases, the materials were shaken strongly. The ability to move freely inside the tube was grouped as lamellar (L_α). It happened due to the layer structure of the lamellar. Where it has a two-dimensional degree of freedom by sliding along with the layer structures. Meanwhile, during shaking H_α-phase was stuck in the fixed position due to the compact structure. Therefore, the two phases were distinguished by observing the flexibility of materials in the shaking process.

2.2 Gelation process

TEOS and ethanol were added to a w/o microemulsion with a TEOS to water molar ratio of 1 : 8, then homogenized with a vortex mixer for about 15 minutes until the formation of sol. It was then heated in a water bath at 65 °C for 6 hours to form a gel.

2.3 Solubility studies of inorganic red and blue pigments in the gelation of water-in-oil microemulsion

The blue pigment was freshly prepared by taking the precipitate of $Fe_2Fe(CN)_6$, resulting in the reaction of 50 ml of $K_4[Fe(CN)_6]$ 1 M and 50 ml of $FeSO_4$ 2 M. The red pigment was prepared by adding 50 ml of $Fe(NO_3)_3$ 1 M to 50 ml of KSCN 3 M. Then, the red solution of $Fe(CNS)_3$ was collected.

The solubility test for the red and blue inorganic pigments was performed by adding each inorganic pigment sample to the w/o-μE. The addition was conducted by adding the inorganic pigment gradually until it could no longer be dissolved in the sample.

2.4 Solubility studies of inorganic yellow and black pigments in the gelation of water-in-oil microemulsion

The yellow pigment was prepared by reacting a 1 M solution of $CaCl_2$ and H_2S gas, where the H_2S gas was produced in a process in which FeS metal was mixed with 3 M HCl in Kipp's apparatus. This reaction produced a yellow precipitate of CdS and was used as a yellow pigment. Meanwhile, to produce black pigments, a 1 M of $CuSO_4$ solution was reacted with H_2S. A black CuS precipitate was then produced and used as the black pigment.

The solubility test for inorganic yellow and black pigments was performed by adding each inorganic pigment sample to the

w/o-μE-gel. The addition was made by adding the inorganic pigment gradually until it could no longer be dissolved.

2.5 Density measurement

An empty 10 ml pycnometer was weighed before and after adding the gel sample and the pigments. Then, by calculating the mass of loaded gel divided by sample volume, we obtained the density of materials.

2.6 Refractive index measurement

An ABBE refractometer was used to measure the refractive index of the sample.[23] Three sample drops were dropped onto the prism, and then the cap was closed. The light source (Na-lamp) was switched on, and the scale display was set to the refractive index of 1.30. Then the refractive index was measured for the desired sample (the sample's refractive index is obtained when the light–dark image is at the top of the reading scale).

2.7 Turbidity measurement

The cuvette was cleaned and dried thoroughly before measurement, and 10 ml of the sample was added to the cuvette. The cuvette was inserted into the turbidimeter apparatus, and the measurements were repeated several times until the result was consistent.

2.8 Stability measurement and prototyping

The ink-encapsulated inorganic pigments in the w/o-μE-gel-was put into the empty ballpoint-pen sleeves and used to write on the paper, and the physical state of the writing was monitored at regular intervals to determine the color fastness of the ink.

3 Result and discussion

First, the titration was used to construct the pseudo ternary phase diagram of water/Tween-60/cyclohexane. The construction of the pseudo ternary phase diagram followed the procedure of Friberg[24] with slight modification. To obtain a pseudo ternary phase diagram of the μE, cyclohexane (C6) was added dropwise to Tw-60 and double-distilled (DD) water mixture and vortex-mixed until homogeneous. From visual observation, the transparent/one-phase liquid was considered as μE. By varying weight ratios, pseudo ternary phase diagrams were plotted, and the μE area was calculated using Origin® software. Calculating the μE area in the pseudo ternary graph was used to obtain the composition and the weight ratio of the components in the mixture. The area of μE was obtained and eqn (1) was used to obtain the percentage area in the pseudo ternary phase diagram.[23]

3.1 Pseudo-phase diagram and phase area

Fig. 2 shows the phase diagram of the Tw-60/C6/water system. The μE-area range extended along the composition line from 100% of C6 to 100% of Tw-60. The w/o-μE area was found in the shallow water content from 0% of water composition at 100% C6 to about 23% of water component at the weight fractions of

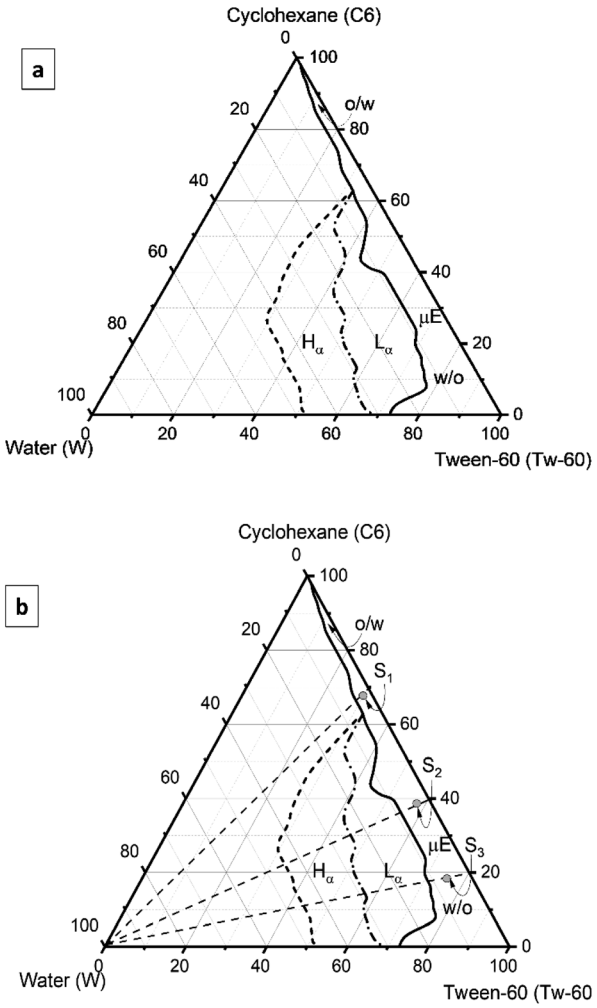

Fig. 2 (a) Pseudo-phase area of microemulsions (μE), lamellar liquid crystals (L_α), and hexagonal liquid crystals (H_α) for water – Tw-60 – cyclohexane systems, and (b) sample points of microemulsions (μE) for inorganic pigments solubility test.

water and Tw-60 line. The μE area started to form at 3% of Tw-60 and 1% of water components to 82% of Tw-60 and 27% of water components. The lamellar liquid crystal (L_α) area began to form at the Tw-60 composition containing 31% of Tw-60 and 11% of water components to a composition containing 81% of Tw-60 and 17% of water components, respectively. Hexagonal liquid crystals (H_α) area began to form at 21% of Tw-60 and 15% of water components to 79% of Tw-60 and 52% of water components. Even though Tw-60 was identified as a non-ionic surfactant, from Fig. 1. Molecular Structure of Tween-60 (Tw-60) could be inferred that the hydrophobic group in Tw-60 could be a stearate group with a longer carbon chain. This longer carbon chain allows Tw-60 to dissolve more onto nonpolar groups, making cyclohexane more soluble in Tw-60.

The complete description of the phase area of the Tw-60/C6/water system is well described in Fig. 2a.

In Fig. 2b, the sample areas were chosen to conduct the solubility test. The points were named S_1, S_2, and S_3. All sample points have similar water compositions but different Tw-60 and

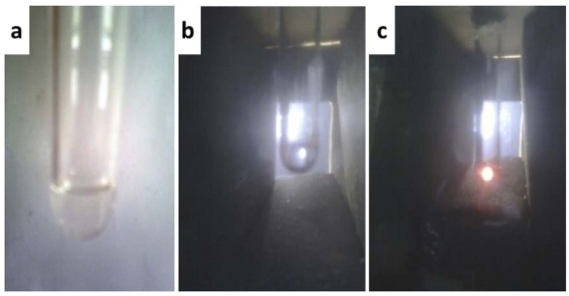

Fig. 3 (a) Microemulsion illuminated under unpolarized white light, (b) microemulsion illuminated under polarized (between two perpendicular polarizers) white light, and (c) liquid crystals illuminated under polarized (between two perpendicular polarizers) white light.

C6 compositions. In our experience, the gelation process was hardly determined by water composition rather than surfactant and co-surfactant (cyclohexane). Hence, representative of one dedicated sample point is enough to figure out essential information of the graph. Nevertheless, in the subsequent description, the sample point means S_3, representing all sample points.

Phase determination was conducted by visual observation and also by parafilm. Physically, a microemulsion area was transparent with low viscosity, while an emulsion was cloudy. Parafilm was used to distinguish between liquid crystals from microemulsions and/or emulsions. Liquid crystal samples look brighter under parafilm, while microemulsion and emulsion samples look faint, as shown in Fig. 3. Parafilm acts as a polarizer and changes the direction of in-plane polarization of visible light.

Two parafilm were used for this purpose, acting as polarizers and analyzers. The incident light was passed through the sample, and the observer could show the brightness or color change from the other side. Liquid crystal materials show strong emissions which could be distinguished by the naked eye.

The two types of liquid crystals in the present work: are lamellar/smectic (L_α) and hexagonal liquid crystals (H_α). These two types of liquid crystals can be distinguished by their properties when stirred with a vortex mixer. L_α-liquid crystals have lower viscosity and can be stirred vigorously using a vortex mixer, while H_α-liquid crystals have a higher viscosity and cannot be stirred easily by using a vortex mixer. Due to this property, both liquid crystalline phase structures could be distinguished.

The sol–gel method was used for gelating w/o-μE. The sol–gel method prepares inorganic silica compounds by chemical reactions in the solution at low temperatures. The sol–gel method involves a phase change from a colloidal suspension (sol) to a continuous liquid phase. Sol is a suspension of colloidal particles (nanoparticles) that are stable in the liquid form. The process of sol formation occurs when TEOS is added to a w/o-μE to form a silica matrix during the gelation process. The interaction between the hydroxyl and ethoxy groups in TEOS was more robust and was challenging to break.

In this work, yellow pigment (CdS) was prepared from the reaction of $CdCl_2$ and H_2S precursors according to eqn (2):

$$CdCl_2 + H_2S \rightarrow CdS + 2HCl \quad (2)$$

The red pigment $[Fe(SCN)_3]^{-2}$ was prepared from the reaction of $Fe(NO_3)_3$ and KSCN precursors according to eqn (3).

$$Fe(NO_3)_3 + 3KSCN \rightarrow [Fe(SCN)_3]^{-2} + 3KNO_3 \quad (3)$$

The blue pigment $Fe_2[Fe(CN)_6]$ or Prussian blue was prepared from the $FeSO_4$ and $K_4[Fe(CN)_6]$ precursors according to eqn (4).

$$2FeSO_4 + K_4[Fe(CN)_6] \rightarrow Fe_2Fe(CN)_6 + 2K_2SO_4 \quad (4)$$

The CuS (black pigment) was synthesized from the $CuSO_4$ precursor according to eqn (5).

$$CuSO_4 + H_2S \rightarrow CuS\downarrow + H_2SO_4 \quad (5)$$

In our experiment, the best proportion of adding TEOS/ethanol to a w/o microemulsion was at a molar ratio of 1 : 8 because it gives optimal yields. The addition of TEOS and ethanol resulted in turbid, viscous, and denser structures compared with stand-alone precursors. The method started with sol formation, where the sol was mixed using a vortex mixer until the turbidity disappeared and the clear transparent liquid was formed.

$$Si(OR)_{4(aq)} + 2H_2O_{(aq)} \rightarrow SiO_{2(aq)} + 4ROH_{(aq)} \quad (6)$$

The reaction continued with the gelation process when the silica matrix was formed when the ethoxy group of TEOS reacted with water molecules to form hydroxyl-substituted intermediates. TEOS was then hydrolysed by adding organic solvents such as ethanol to form silanol (Si–OH), followed by a condensation process in which the silanol group transformed into a siloxane group.

During gel formation, the initial TEOS concentration was inversely proportional to the size of the particles. The higher TEOS concentration leads to smaller particle size, reducing the solution density and increasing viscosity. A gel is a colloidal mixture with two distinct phases, solid and liquid—concentration and temperature influence the gel formation process. The gel was formed at 65 °C by hydrolysis and condensation of cross-links. The heating process lasts 6–12 hours and results in a semi-solid gel with a soft, chewy/rubbery, and transparent.[25]

3.2 Solubility studies of inorganic pigments in the microemulsion sols (μE-sol)

Solubility of inorganic pigments in the μE-sol can simply be summarised in Table 1.

Solubility of inorganic pigments ($\mathbb{S}$) for black, yellow, red, and blue are $2.9 < \mathbb{S} > 3.6$ (mg g^{-1}). The highest solubility value is given by $Fe(CNS)_3$ (red pigment), whereas the lowest solubility is given by CdS (yellow pigment).

The solubility of inorganic pigments can be explained by the solubility of salts solution in the microemulsions.[26] Solubility of $[Fe(SCN)_3]^{-2}$ (red), $Fe_2Fe(CN)_6$ (blue), and CuS (black) were relatively the same because the cation size of Fe^{2+} (78 pm), Fe^{3+} (69 pm), and Cu^{2+} (73 pm) of the salts are relatively the same. Whereas the solubility of CdS was relatively lower because the

Table 1 Solubility, density, refractive indices, and turbidity of sol after being introduced by inorganic pigments

Sample (S)	Maximum solubility ($\mathbb{S}$) mg g^{-1}	Density (ρ)[a] g cm^{-3}	Refractive indices (n)	Turbidity (θ) NTU
Black	3.22 ± 0.05	0.924 ± 0.05	1.4331 ± 0.05	1.90 ± 0.05
Yellow	2.92 ± 0.05	0.915 ± 0.05	1.4225 ± 0.05	1.87 ± 0.05
Red	3.63 ± 0.05	0.960 ± 0.05	1.4360 ± 0.05	1.89 ± 0.05
Blue	3.21 ± 0.05	0.922 ± 0.05	1.4149 ± 0.05	1.85 ± 0.05

[a] ρ^{θ}: 0.82 g cm^{-3}, n^{θ}: 1.4074, θ^{θ}: 1.80 NTU, according to Indonesian National Standard (SNI) No. 06-1567-1999, the density of commercial ink should between 0.9–1.0 g cm^{-3} (Renggains, *et al.*, 2017). The uncertainty values is determined using 95% significance value for 3-sample points S_1, S_2, and S_3.

cation size Cd^{2+} (95 pm) is slightly bigger than the other three cations. Our observation is in agreement with research conducted by Chai, *et al.*,[27] where the authors confirmed the effect of cation size ($MgCl_2$, $CaCl_2$, and $SrCl_2$) on the solubility of oil in w/o microemulsions. The hydrated radii could explain the cation effect; large cation tends to have more hydrated radii, resulting in more challenges to fight against the hydrophilic environment. A similar effect might be attributed to anion size. In the protein solubility study, SCN^- anion demonstrated the exceptional ability to dissolve due to strong interaction with the amide backbone of proteins. These dissolution properties have similar characteristics to the solubility of our system.[28]

The addition of inorganic pigments into the microemulsions increased the microemulsions' density, refractive index, and turbidity. The number of added materials corresponded with the enhanced physical properties of microemulsions, such as density, refractive index, and turbidity ($c \propto \rho \propto n \propto \theta$). As presented in Table 1, the maximum density was given by red inorganic pigment as well as refractive index and turbidity.[29] It could be explained; because the number of materials added to the system was higher, resulting in an increasing number of components. On the other hand, the lowest density, refractive index, and turbidity were given by yellow pigments.[30] It was due to the quantity of added materials to the system being much lower.

The μE-gel's physical appearance after pigment addition is presented in Fig. 4. Each pigment demonstrated good solubility in the μE-sol, and after homogeneously mixing, the microscopic mixture shows excellent stability.

3.3 Prototype design and stability

The ballpoint prototype design was illustrated in Fig. 5. Some quantities of encapsulated inorganic pigment in w/o-μE was inserted in the pen's sleeve and used as writing ink. The results show that the inorganic pigment in μE-gel performs well, as well as a regular ink pen. For blue pigment, the writing shows a solid Prussian blue color.[31] Although the time for solvent evaporation was a bit longer, compared with the commercial blue pen, in general, the result was satisfactory. The red, yellow, and black pigment demonstrated a solid color as well as Prussian blue, but the color stability was not as good as Prussian blue.[32] Notably, the black ink gradually fainted after three days of exposure to air. Nevertheless, comprehensive research should be conducted to understand the inks' stability properties fully.

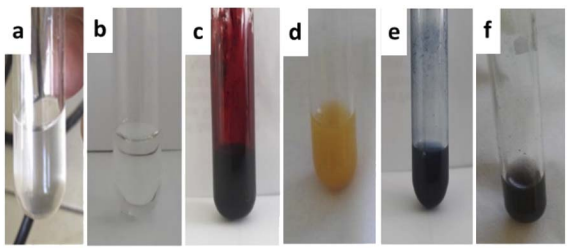

Fig. 4 (a) o/w μE, (b) sol, (c) red pigment in sol, (d) yellow pigment in sol, (e) blue pigment in sol, (f) black pigment in sol.

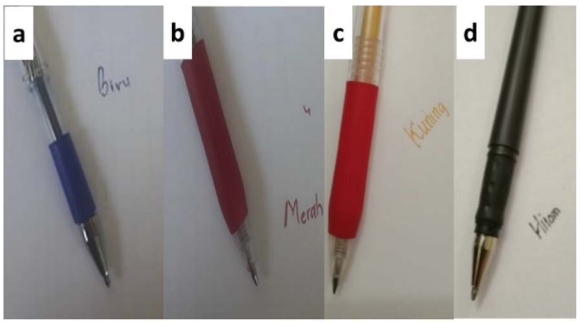

Fig. 5 The ink prototype of (a) blue, (b) red, (c) yellow, and (d) black.

4 Conclusions

The pseudo-phase diagram of Tween-60/cyclohexane/water was used to map w/o-microemulsion, lamellar/smectic liquid crystals, and hexagonal liquid crystals. A given composition sample of w/o microemulsion area was used to study the solubility of inorganic pigments $[Fe(SCN)_3]^{-2}$ (red), $Fe_2Fe(CN)_6$ (blue), CdS (yellow), and CuS (black). The result shows that the highest solubility value was given by $Fe(CNS)_3$ (red pigment) of 3.65 ± 0.05 mg g^{-1}, whereas the lowest solubility was given by CdS (yellow pigment) of 2.92 ± 0.05 mg g^{-1}. Meanwhile, for Fe_2-$Fe(CN)_6$ (blue), and CuS (black), the solubility was ~3.2 ± 0.05 mg g^{-1}. The solubility difference is due to the cation and anion size, where the more extensive of the cation/anion, the bigger the hydrated radii, resulting in challenges to diluting in the microemulsion system. Furthermore, some quantities of pigments encapsulated in microemulsion gel have been

inserted into the ballpoint sleeves as a prototype, and the demonstration shows that it could be used as a ballpoint ink. Finally, research on the stability of the ink under light, temperature, oxidation, and chemical need to be conducted more to understand the physico-chemical properties of inorganic salts solubility in microemulsion gels.

Author contributions

DB: conceptual – planning, lab experiments, writing – original draft, writing – review & editing, methodology, formal analysis; SB, NYS, FY, EE: lab experiment, working on characterization, AA: conceptual, writing – review & editing, methodology, formal analysis, visualization, project administration, & resources; GG: formal analysis, project administration, & resources.

Conflicts of interest

The authors have no conflicts to declare.

Acknowledgements

AA and DB, thanks to skema grant penelitian guru besar LPPM Universitas Negeri Padang No.: 983/UN35.13/LT/2022. DB, SB, and AA, thanks to Chemistry Department's Laboratory for the research facility and equipment. All authors thank Universitas Negeri Padang for the research grant, facility, and equipments.

Notes and references

1 X. Zhou and J. Hao, Solubility of NaBr, NaCl, and KBr in Surfactant Aqueous Solutions, *J. Chem. Eng. Data*, 2011, **56**(4), 951–955.
2 V. Pauk, J. Michalčáková, K. Jagošová and K. Lemr, Origin of indigo colorants revealed by ion mobility spectrometry coupled to mass spectrometry followed by supervised classification, *Dyes Pigm.*, 2022, **197**, 109943.
3 C. Jung, J. I. Rhee, D. I. Yoo and Y. Shin, Application of Fluorescence Spectroscopy in Indigo Reduction Process: Identification of Reduction Stages and Reduced Indigo Concentration, *Fibers Polym.*, 2022, **23**(1), 127–135.
4 J. Fang, C. Meng and G. Zhang, Agricultural waste of Ipomoea batatas leaves as a source of natural dye for green coloration and bio-functional finishing for textile fabrics, *Ind. Crops Prod.*, 2022, **177**, 114440.
5 W. Shi, T. Li, Y. Tian, H. Li, M. Fan, H. Zhang and X. Qin, An innovative hollow fiber vacuum membrane distillation-crystallization (VMDC) coupling process for dye house effluent separation to reclaim fresh water and salts, *J. Cleaner Prod.*, 2022, **337**, 130586.
6 M. Li, H. Zhang, Z. Wu, Z. Zhu and X. Jia, DPD Simulation on the Transformation and Stability of O/W and W/O Microemulsions, *Molecules*, 2022, **27**, 1361.
7 Y. Fu, C. Qin, S. Gao, C. Lv, C. Zhang and Y. Yao, Aquifer flushing using a SDS/1-butanol based in-situ microemulsion: Performance and mechanism for the remediation of nitrobenzene contamination, *J. Hazard. Mater.*, 2022, **424**, 127409.
8 S. Manikandan, R. Subbaiya, M. Saravanan, M. Ponraj, M. Selvam and A. Pugazhendhi, A critical review of advanced nanotechnology and hybrid membrane based water recycling, reuse, and wastewater treatment processes, *Chemosphere*, 2022, **289**, 132867.
9 E. Breniaux, P. Dufour, J. Esvan, S. Mallet-Ladeira, A. Balocchi and C. Tenailleau, Spontaneous moisture-driven formation of Cs2Pb1-xMxCl2I2 single crystals with M = Bi, In, Ga and Cr, *J. Cryst. Growth*, 2022, **584**, 126584.
10 W. An, P. He, Z. Che, C. Xiao, E. Guo, C. Pang, X. He, J. Ren, G. Yuan, N. Du, D. Yang, D. L. Peng, Q. Zhang, *et al.*, Scalable Synthesis of Pore-Rich Si/C@C Core–Shell-Structured Microspheres for Practical Long-Life Lithium-Ion Battery Anodes, *ACS Appl. Mater. Interfaces*, 2022, **14**(8), 10308–10318.
11 C. Wang, J. Cai, Y. Ye, X. Hu, L. Zhong, H. Xie, E. Chen, Y. Ye, S. Xu, J. Sun, Q. Yan and T. Guo, Full-visible-spectrum perovskite quantum dots by anion exchange resin assisted synthesis, *Nanophotonics*, 2022, **11**(7), 1355–1366.
12 Y.-X. Li, Y. Liu, H. Wang, Z.-T. Li and D.-W. Zhang, Water-Soluble Porphyrin-Based Nanoparticles Derived from Electrostatic Interaction for Enhanced Photodynamic Therapy, *ACS Appl. Bio Mater.*, 2022, **5**(2), 881–888.
13 J. Feng, J. Wang, D. Wang, M. Han, G. Qian, F. Wu, Q Lin and Z. Hu, Reversible Phase Transitions of all Inorganic Copper-Based Perovskites: Water-Triggered Fluorochromism for Advanced Anticounterfeiting Applications, *ACS Appl. Electron. Mater.*, 2022, **4**(1), 225–232.
14 J. A. Adewuyi, N. D. Schley and G. Ung, Synthesis of bright water-soluble circularly polarized luminescence emitters as potential sensors, *Inorg. Chem. Front.*, 2022, **9**, 1474–1480.
15 Y. Zhang, *et al.*, Inorganic salts in sub-/supercritical water—Part A: Behavior characteristics and mechanisms, *Desalination*, 2020, **496**, 114674.
16 L. Zhong, J. Ding, J. Qian and M. Hong, Unconventional inorganic precursors determine the growth of metal-organic frameworks, *Coord. Chem. Rev.*, 2021, **434**, 213804.
17 X. Feng, D. Peng, J. Zhu, Y. Wang and Y. Zhang, Recent advances of loose nanofiltration membranes for dye/salt separation, *Sep. Purif. Technol.*, 2022, **285**, 120228.
18 R. Muñoz-Espí and O. Álvarez-Bermúdez, Application of Nanoemulsions in the Synthesis of Nanoparticles, in *Nanoemulsions*, ed. S. M. Jafari and D. J. McClements, Academic Press, 2018, chapter 15, pp. 477–515.
19 R. Swartwout, M. T. Hoerantner and V. Bulović, Scalable Deposition Methods for Large-area Production of Perovskite Thin Films, *Energy Environ. Mater.*, 2019, **2**(2), 119–145.
20 D. Yu, Z. Xue and T. Mu, Eutectics: formation, properties, and applications, *Chem. Soc. Rev.*, 2021, **50**(15), 8596–8638.
21 F. Talavar, A. Soleimani-Gorgani, M. Ghahari and R. Jafari, Water-based ink-jet ink based on nano Ni and Sb doped TiO2 prepared for printing on ceramics, *J. Asian Ceram. Soc.*, 2021, **9**(1), 382–392.

22 Q. Wang, Y. Wang, Q. Chang, H. Liu, Y. Yang and X. Zhang, Preparation of Ultrafine Spherical Pr-ZrSiO4 Pigment by Sol-Gel-Microemulsion Method, *Silicon*, 2020, **12**(3), 585–594.
23 G. Lu, G. Wenzhi, L. Zhengchun, C. Tianying and C. Hongliang, SPR principle refractive index testing system for offshore oil spill, *J. Infrared and Laser Engineering*, 2019, **48**(8), 813006.
24 S. E. Friberg, Applications of amphiphilic association structures, *Adv. Colloid Interface Sci.*, 1990, **32**(2), 167–182.
25 A. Froelich, T. Osmałek, P. Kunstman, B. Jadach, M. Brzostowska and W. Białas, Design and study of poloxamer-based microemulsion gels with naproxen, *Colloids Surf., A*, 2019, **562**, 101–112.
26 E. B. Abuin, M. A. Rubio and E. A. Lissi, Solubility of Water in Water-in-Oil Microemulsions Stabilized by Cetyltrimethylammonium: Effects of the Surfactant Counterion, the Nature and Composition of the Oil, and the Salinity of the Droplets, *J. Colloid Interface Sci.*, 1993, **158**(1), 129–132.
27 J. L. Chai, H. Sun, X. Q. Li, L. S. Chen, B. Yang and Y. T. Wu, Effect of Inorganic Salts on the Phase Behavior of Microemulsion Systems Containing Sodium Dodecyl Sulfate, *J. Dispersion Sci. Technol.*, 2012, **33**(10), 1470–1474.
28 K. D. Collins, The behavior of ions in water is controlled by their water affinity, *Q. Rev. Biophys.*, 2019, **52**, e11.
29 A. Alam, *et al.*, A microemulsion-based gel of isotretinoin and erythromycin estolate for the management of acne, *J. Drug Delivery Sci. Technol.*, 2022, **71**, 103277.
30 A. Kajbafvala and A. Salabat, Microemulsion and microemulsion gel formulation for transdermal delivery of rutin: Optimization, in-vitro/ex-vivo evaluation and SPF determination, *J. Dispersion Sci. Technol.*, 2021, 1–16.
31 A. Hase, Evaluation of Writing Performance for Different Types of Ballpoint Pen Ink by Acoustic Emission Sensing, *Lubricants*, 2022, **10**, 44.
32 B. Łydżba-Kopczyńska, T. Czaja, R. Cieśla and G. Rusek, Application of chemometric methods for the determination of fading and age determination of blue ballpoint inks, *J. Raman Spectrosc.*, 2021, **52**(1), 159–169.